Ultrastable carbazole-tethered conjugated microporous polymers for high-performance energy storage

Mostafa Ahmed [a], Mohammed G. Kotp [b], Tharwat Hassan Mansoure [c], Rong-Ho Lee [d], Shiao-Wei Kuo [b], Ahmed F.M. EL-Mahdy [b,c,*]

[a] *Chemistry Department, Faculty of Science, New Valley University, El-Kharja, 72511, Egypt*
[b] *Department of Materials and Optoelectronic Science, National Sun Yat-Sen University, Kaohsiung, 80424, Taiwan*
[c] *Chemistry Department, Faculty of Science, Assiut University, Assiut, 71516, Egypt*
[d] *Department of Chemical Engineering, National Chung Hsing University, Taichung, 402, Taiwan*

ARTICLE INFO

ABSTRACT

Conjugated microporous polymers (CMPs) have considered as organic porous polymers featuring combination of *p*-conjugated skeletons with permanent micro-porosity. In the present study, we report the synthesis of carbazole-tethered conjugated microporous polymers, BC-Py-CMP and BC-BF-CMP, respectively, through the Suzuki-Miyaura coupling polymerization of the novel 3,3′,6,6′-tetraboronic-pinacolate-9,9′-bicarbazole (BC-4Bpin) with 1,3,6,8-tetrabromopyrene (Py-4Br) and 3,3′,6,6′-tetrabromo-9,9′-bifluorenylidene (BF-4Br). These CMPs exhibited extraordinary thermal stabilities (up to ca. 694 and 569 °C) and high surface areas (up to ca. 1030 m^2 g^{-1}). Moreover, the as-prepared BC-BF-CMP exhibited a high specific capacitance of 260 F g^{-1} at 0.5 A g^{-1} and showed outstanding cycling stability, having 89.60% capacitance retention of its authentic capacitance over 6000 cycles. The excellent electrochemical capacitances of the BC-BF-CMP were presumably due to the 9,9′-BF could easily accept one electron, causing the reduced form acquiring greater aromaticity by meeting Huckel's requirements, as a result improving the electron transporting properties. Such CMPs tend to have tremendous potential to be used as a high-performance supercapacitors in energy storage systems.

1. Introduction

Framing materials such as organic frames (covalent organic frameworks and triazine organic frameworks) and inorganic frames (mesoporous silica, and metal organic frameworks) are porous materials [1–12]. The advantages presented by porous materials led chemists to employ such kinds of materials in invested fields and novel industries as a result of their remarkable features such as high surface area, unblock channels in addition to controlling the pore sizes [3]. A rising interest has been paid to the porous polymer category due to their capability to merge the merits of polymers as well as porous materials [3,6,7,13]. Chemical variety in addition to ease of processing are the master merits of porous polymers over many porous substrates. The chemical formation in porous organic polymers was found to be through strong covalent bonds and showed a high surface area and low mass density [2–7]. Porous polymers were applied as ion exchange resins for pharmaceutical application [14], environment protection [15] as well as food packing [16]. Most recently porous polymers were used in energy storage

devices such as supercapacitors, in addition to other applications [17–27].

Cooper and co-workers [28] documented a new family of porous organic polymers called π-conjugated microporous polymers (CMPs). Conjugated microporous polymers fabricated from a very broad range of building blocks starting from very simple phenyl units, heterocyclic aromatics to large macromolecules. This variety of building blocks made CMPs are promising platforms for a new generation of porous material science [29–31]. In addition, CMPs have no restrictions on size, geometry as well as function groups that why they are capable of turning their π conjugated porous structures as well as permit reaching to definite features [32]. CMPs are also discriminated rather than the major organic porous polymers by their high electron delocalization through their network structures which enhance energy absorption as well as charge movement [32,33]. The Yamamoto [34], Suzuki coupling [35], Sonogashira−Hagihara coupling [36], ethynyl trimerization [37,38], Schiff-base condensation reactions [39] were applied for the fabrication of conjugated microporous polymers. Among CMPs, nitrogen-contained

conjugated polymers have received much attention from researchers due to their intrinsic photoelectric characters [40]. Carbazole is a nitrogen-contained moiety and has a focused interest for the fabrication of highly porous organic polymers [41]. The high aromaticity, as well as the excellent physicochemical stability of carbazole units, are due to the rigid skeleton and the high connectivity of carbazole [42,43]. The rigidity of polycarbazoles stood up well to the high thermal and chemical environment. The electron-rich through porous carbazole polymer was due to the existence of polar NH group which played an important role in various applications. It worth mentioning that carbazole polymers are economic, full aromatic property as well as ease of modification, therefore carbazole polymers have been applied for several interesting applications such as sensing, energy storage, solar cells, photo refractive materials, and light-emitting diodes [44–52].

Energy storage devices such as supercapacitors gained great interest nowadays [53]. The high power density, stable long cycle of the supercapacitor, high rate of charge-discharge as well as environment favoring have a great effect onto their rate execution as well as energy density [54–57]. Ion adsorption onto electrode surface is the main power for storing energy through electrochemical double layer (EDL). It is aforementioned that the stored energy is maximized within high-porous electrodes [58–65]. On the other hand, fast and reversible redox reactions allow energy to be stored via pseudocapacitance [66]. To combine the synergistic effect between both types EDL and pseudocapacitance are highly required to design an electrode tended to ideality. The electrode tends to be ideal if the following features are available high surface area, high electrical conductivity, proper pores, high thermal stability, and chemically stable. CMPs represented proper electrical double layer features and their energy storage as supercapacitors could be followed one of the following twice avenues; the EDL through the surface of CMPs, and the other is the faradaic reaction between electrolyte and redox moieties [67]. In EDL-based supercapacitors, CMPs have been widely used because the extended

π-conjugated structure along their backbones which provided superior physicochemical stability, large surface area, and robust porous structure. In addition, the high surface area and crosslinked structure of CMPs offered greater pore spaces for carriers and larger contact surface areas for shortening ion diffusion distance, assuring excellent electrochemical stability, activity, and rapid kinetic [62–65]. On the other hand, the preparation of new CMPs possess redox-active units and high surface areas remain much opportunity for development. Previously, costly materials were utilized for such systems, but conjugated polymers combine functionality with cost effectiveness. For example, polyaniline nanostructures electrode was fabricated by Wang and coworkers et al. [68] and showed one of the highest polymer-based electrode capacitances around 1221 F g^{-1}.

However, such kinds of conjugated polymers suffer from bit disadvantages as non-durability as a result of decomposition after charge-discharge cycles due to swelling and shrinkage of linear macromolecular structure. In addition, to the best of our knowledge, the use of 3,3′,6,6′-tetraboronic-pinacolate-9,9′-bicarbazole (BC-4Bpin) as redox-active unit to prepare CMP has not been reported previously. Therefore, in this study, Suzuki-Miyaura coupling polymerization of the novel BC-4Bpin with 1,3,6,8-tetrabromopyrene (Py-4Br) and 3,3′,6,6′-tetrabromo-9,9′-bifluorenylidene (BF-4Br) was applied for the synthesis of two novel carbazole-tethered conjugated microporous polymers BC-Py-CMP and BC-BF-CMP (Scheme 1). The chemical structures of the resultant CMPs were confirmed using spectroscopic analyses. The surface areas and thermal stabilities of all CMPs were exceptionally high. The as-prepared BC-BF-CMP exhibited a high specific capacitance of 260 F g^{-1} at 0.5 A g^{-1} and showed outstanding cycling stability, having 89.60% capacitance retention of its authentic capacitance over 6000 cycles. As a result, it is a potential material for energy storage applications.
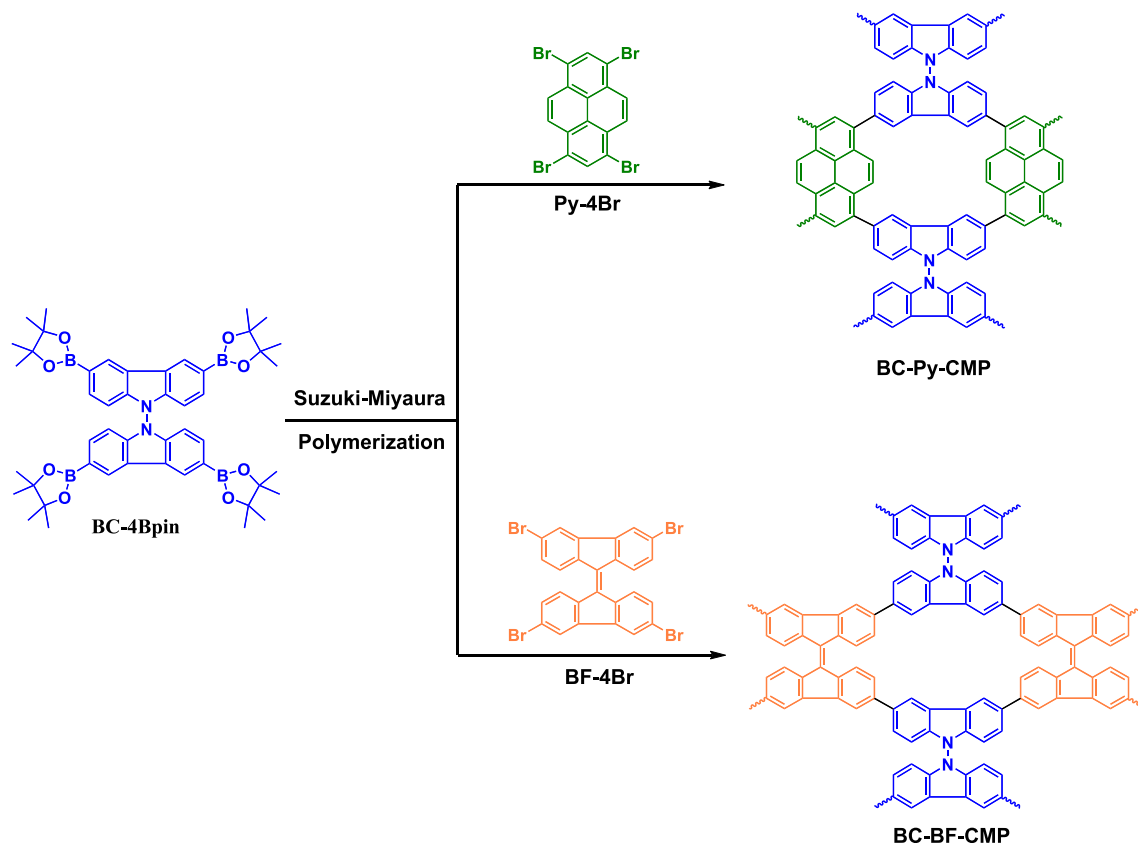
Scheme 1. Schematic strategies for the synthesis of BC-Py-CMP and BC-BF-CMP.

2. Experimental section

2.1. Materials

Chemicals and solvents were obtained from commercial sources and used as received. Pyrene, tetrakis(triphenylphosphine)palladium(0), *N*-Bromosuccinimide, and carbazole were purchased from Across. Phenanthrene-9,10-dione, dibenzoyl peroxide, potassium permanganate, and Lawesson's reagent were obtained from Alfa Aesar. Bis(pinacolato)diboron, potassium carbonate, and potassium acetate were purchased from J. T. Baker. Bromine, nitrobenzene, and sulfuric acid were obtained from Sigma–Aldrich.

2.2. General synthesis of CMP

A mixture of tetrabromo-linker (0.239 mmol, Schemes S1-S3), 3,3′,6,6′-tetraboronic-pinacolate-9,9′-bicarbazole (200 mg, 0.239 mmol, Scheme S4), tetrakis(triphenylphosphine)palladium(0) (0.025 mmol), and K_2CO_3 (2.39 mmol) were added into a Pyrex tube (25 mL) and subjected to a vacuum for 15 min. DMF (10.34 mL) and H_2O (1.34 mL) were added then degassed using three freeze/pump/thaw cycles. The tube was flame-sealed and heated at 150 °C for 3 days. After the tube had cooled to room temperature, the precipitate was filtered out and rinsed with methanol. To obtain the CMP, the solid was vacuum dried overnight at 120 °C (Schemes S5 and S6).

3. Results and discussions

Carbazole is an aromatic nucleus with extreme stability towards thermal, chemical, and environmental influences. Due to the excellent charge-transporting capability of carbazole, recently numerous carbazole-based materials have received prominence for use in several applications including energy storage and electronic devices [44–52]. To avail these desirable features of carbazole, we constructed a new carbazole-based monomer (BC-4Bpin) for the synthesis of two carbazole-based conjugated microporous polymers, then estimated the energy storage performance of these polymers. The new precursor tetraboronic-pinacolate(BC-4Bpin) was synthesized in an excellent yield as shown in synthetic route in Scheme S4, through the reaction of 3,3′,6,6′-tetrabromo-9,9′-bicarbazole (BC-4Br) with bis(pinacolate)diboron in dry 1,4-dioxane in the presence of [1,1′-bis(diphenylphosphino)ferrocene] dichloropalladium(II) as a catalyst to facilitate the process of displacement of bromide and potassium carbonate as a base catalyst at 150 °C under nitrogen atmosphere. The chemical structure of the BC-4Bpin was established based on spectral analysis including Fourier transform infrared (FTIR) and nuclear magnetic resonance (NMR). The FTIR showed characteristic absorption bands in the range 2929–2977 cm^{-1} for C–H aliphatic, 1602 cm^{-1} for C=C bond, 1147 cm^{-1} is due to B–O asymmetric stretching and characteristic band at 1080 cm^{-1} due to C–N asymmetric stretching (Fig. S1). The ^1H NMR spectrum of BC-4Bpin was characterized by the appearance of a new singlet signal at 1.32 ppm due to the methyl groups and three signals at 6.80 (doublet), 7.71 (doublet), and 8.70 (singlet) ppm for the aromatic protons (Fig. S2). The ^{13}C NMR spectrum of BC-4Bpin was exhibited four characteristic signals at 141.65, 133.11, 88.47, and 24.16 ppm attributed to the C–N, C–B, C–O, and methyl carbons (Fig. S3). All these findings confirmed the formation (BC-4Bpin) and the incorporation between (BC-4Br) and bis(pinacolate)diboron. Then, the 3,3′,6,6′-tetraboronic-pinacolate-9, 9′-bicarbazole (BC-4Bpin) on hand was used as a precursor material to synthesis two novel conjugated microporous polymers—BC-Py and BC-BF-CMPs—using Suzuki–Miyaura reactions. Coupling of BC-4Bpin with 1,3,6,8-tetrabromopyrene (Py-4Br), which prepared according to previous procedure [25], in a co-solvent of DMF and water (1:0.1, v/v) in the presence of [1,1′-bis(diphenylphosphino) ferrocene] dichloropalladium(II) as a catalyst and potassium carbonate as a base catalyst afforded the BC-Py-CMP as a green solid in an excellent yield. On the

other hand, the coupling of BC-4Bpin with 3,3′,6,6′-tetrabromo-9, 9′-bifluorenylidene (BF-4Br), which prepared according to previous procedure [25], in a co-solvent of DMA and water (1:0.1, v/v) in the presence of [1,1′-bis(diphenylphosphino) ferrocene] dichloropalladium (II) as a catalyst and potassium carbonate as a base catalyst gave the corresponding BC-BF-CMP as a red solid in an excellent yield as shown in Scheme 1. The assignment of chemical structures for both polymers—BC-Py-CMP and BC-BF-CMP—were elucidated by spectral analysis. As shown in Fig. 1a, the FTIR spectra of BC-Py-CMP showed a characteristic absorption band at 3036 cm^{-1} for the stretching C–H aromatic groups, in addition to absorption bands at 1601,1471 and 1449 cm^{-1} for C=C bonds and disappearance the bands in the range 2929–2977 cm^{-1} which representing to C–H stretching aliphatic, and band at 1147 cm^{-1} for the B–O asymmetric stretching which existing in the precursor material monomer (BC-4Bpin). The solid-state ^{13}C CP/MAS NMR measurement of the BC-Py-CMP exhibited characteristic signals appeared in the range from 145.64-135.56, 134.06–117.92, and 114.40–105.06 ppm for the carbon atoms in the aromatic rings (Fig. 2). On the other hand, the FTIR spectrum which recorded for BC-BF-CMP featured a characteristic absorption band at 3045 cm^{-1} for the stretching C–H aromatic groups, in addition to absorption bands at 1599,1467 and 1435 cm^{-1} for C=C bonds and disappearance the bands at 2929–2977, and 1147 cm^{-1} for the C–H stretching aliphatic protons and B–O asymmetric stretching, respectively (Fig. 1b). The solid-state ^{13}C CP/MAS NMR measurement of the BC-BF-CMP featured characteristic signals in the range from 149.93-136.06, 134.07–115.43, and 112.63–105.33 ppm for the carbon atoms in the aromatic rings (Fig. 2). These results proved the incorporation between BC-4Bpin and the two monomers—Py-4Br and BC-4Br—to produce the BC-Py-CMP and BC-BF-CMP, respectively.

Thermal stability of our synthesized CMPs was investigated by measuring thermal gravimetric analysis (TGA), as shown in Fig. 3. Our synthesized polymers were heated under nitrogen atmosphere from 100 °C to 1000 °C with a heating rate of 20 °C min^{-1}. BC-Py-CMP and BC-BF-CMP exhibited extraordinary thermal stabilities, with temperatures of 10% weight loss (T_{d10}) of approximately 694 and 569 °C, respectively, and char yields of 61.70 and 57.11%, respectively. The decompositions of BC-Py-CMP and BC-BF-CMP were observed at 725.70 and 721.82 °C with significant weight loss of 26.5% and 31.9%, respectively. These findings indicated that our BC-Py-CMP and BC-BF-CMP have superior thermal stabilities to those of the previously reported conjugated microporous polymers, which decomposed at temperatures below 400 °C. Furthermore, the chemical stability of BC-Py-CMP and BC-BF-CMP in water was studied by immersing 40 mg of each CMP in 100 mL of water for four days, then isolating the CMP using vacuum filtration and drying it under vacuum at 120 °C overnight. As observed in Fig. S4, the exceptional chemical stability of the BC-Py-CMP and BC-BF-CMP in water was demonstrated by the preservation of the FTIR and solid state ^{13}C CP/MAS NMR peaks with no appreciable change after immersion in the water. We then used field emission scanning electron microscopy (FE-SEM) and transmission electron microscopy (TEM) to study the morphologies of our synthesized CMPs. As shown in Fig. 4a–d, the FE-SEM images of BC-Py-CMP and BC-BF-CMP featured uniformly distributed and loose blocks with several hundred nanometer length. The TEM images of BC-Py-CMP and BC-BF-CMP confirmed the distributed loose morphologies of our CMPs (Fig. 4e–h and Fig. S5). The permanent porosities of our synthesized CMPs including, Brunauer–Emmett–Teller (BET) specific surface area, pore size, and pore volume were estimated by measuring the N_2 adsorption/desorption curves of BC-Py-CMP and BC-BF-CMP at −196.15 °C (77 K). As shown in Fig. 5a and b, the two CMPs exhibited adsorption/desorption curves of type IV with a strong N_2 adsorption in the relative pressure (P/P_0) range from 0.0 to 0.1 bar and a brittle increase in the P/P_0 range from 0.1 to 0.9 bar, indicating the microporous structures of BC-Py-CMP and BC-BF-CMP. In addition, the BET specific surface areas and pore volumes of our synthesized CMPs were calculated from their curves, were 1030 m^2 g^{-1} and 0.75 cm^3 g^{-1} for BC-Py-CMP, respectively; for BC-BF-CMP, they
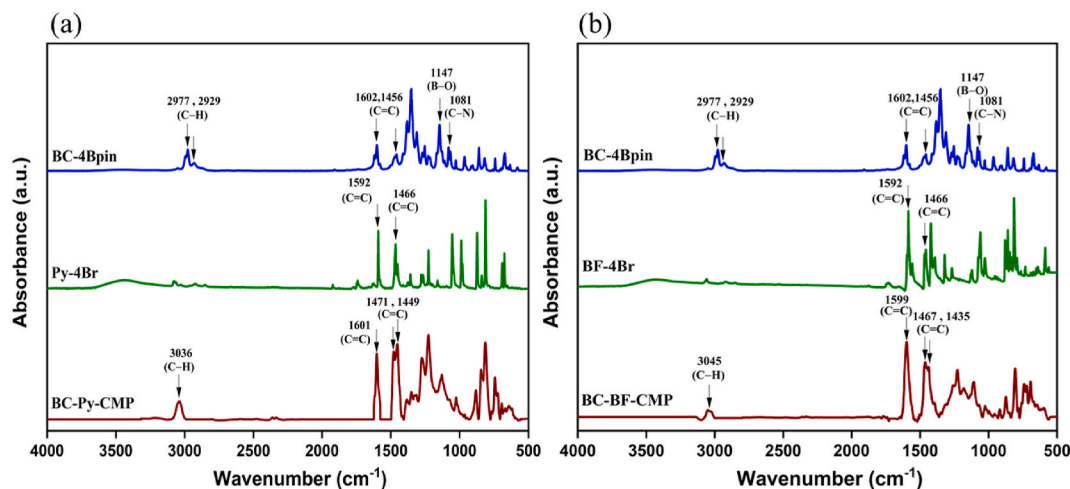
Fig. 1. FTIR spectra of BC-4Bpin (a, and b, blue), Py-4Br (a, olive), BC-Py-CMP (a, wine), BF-4Br (b, olive), and BC-BF-CMP (b, wine). (For interpretation of the references to colour in this figure legend, the reader is referred to the Web version of this article.)
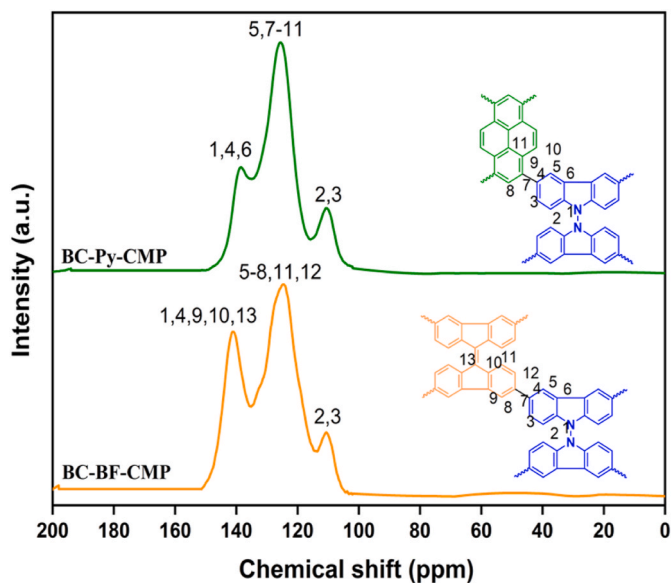

Fig. 2. Solid state ^{13}C CP/MAS NMR spectra of BC-Py-CMP (olive) and BC-BF-CMP (orange). (For interpretation of the references to colour in this figure legend, the reader is referred to the Web version of this article.)

Fig. 3. TGA curves isotherms of BC-Py-CMP (olive) and BC-BF-CMP (orange). (For interpretation of the references to colour in this figure legend, the reader is referred to the Web version of this article.)

were 355 m^2 g^{-1} and 0.32 cm^3 g^{-1}, respectively. We used nonlocal density functional theory (NL-DFT) to calculate the pore sizes of BC-Py-CMP and BC-BF-CMP (Fig. 5c and d). The pore size distribution curves of BC-Py-CMP and BC-BF-CMP revealed the values of pore diameters of 1.67 and 1.88 nm, respectively. The above data suggested that the monomer strut length of the linker strongly affected the BET specific surface area of the CMPs. It has been reported that the BET surface area of CMPs increased as the monomer strut length decreased [69,70]. Consequently, the BC-Py-CMP which obtained from the shorter struts linker (pyrene) exhibited higher BET specific surface area than the BC-BF-CMP which derived from the longer struts linker (bifluorenylidene).

The electrochemical performance of BC-Py-CMP and BC-BF-CMP samples was estimated through cyclic voltammetry (CV) and galvanostatic charge-discharge (GCD) measurements using a three-electrode system in 1 M KOH aqueous solution. Fig. 6a and b displayed the corresponding CV curves of BC-Py-CMP and BC-BF-CMP samples, respectively, measured at various sweep rates ranging from 5 to 200 mV s^{-1}
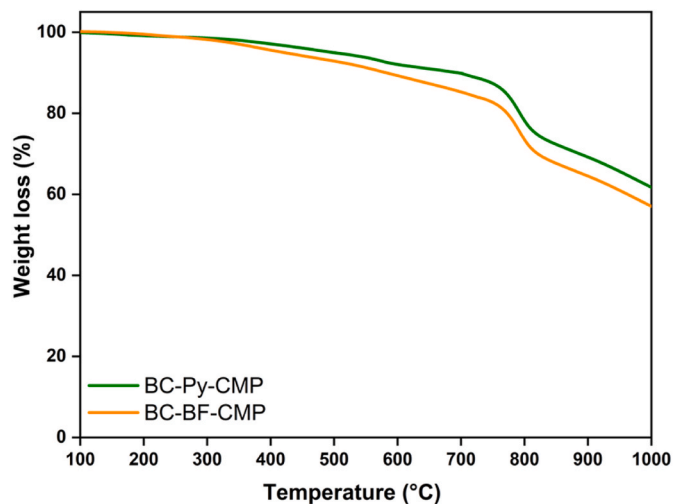
with a potential window ranging from 0 to −1 V (*vs.* Hg/HgO). The BC-BF-CMP provided a relatively higher current density compared to that of BC-Py-CMP. The related CV curves of these CMPs showed rectangle-like shapes, suggesting that the capacitive response mostly caused by the electric double-layer capacitance (EDLC) with minimal pseudocapacitance due to the presence of the electron-rich phenyl rings and nitrogen heteroatoms [18,19,71]. Furthermore, as the sweep rate was raised from 5 to 200 mV s^{-1}, the current density increased but the shape of the CV curves remained same, indicating strong rate capability and simple kinetics [6,7].

Fig. 6c and d presented the GCD curves of the BC-Py-CMP and BC-BF-CMP, respectively, measured at various current densities ranging from 0.5 to 20 A g^{-1}. These GCD curves exhibited triangular forms with a little bend, indicating both pseudocapacity and EDLC properties [10, 11]. The discharging time of the BC-BF-CMP was longer than that of the BC-Py-CMP (Fig. 6c and d), indicating that the capacitance of the BC-BF-CMP was higher than that of the BC-Py-CMP. We used eqn (S1) (ESI) to determine the specific capacitances from the GCD curves (Fig. 7a). Based on the discharge time, the specific capacitance of the BC-BF-CMP (260 F g^{-1}) was larger than that of the BC-Py-CMP (211 F g^{-1}) at a current density of 0.5 F g^{-1}. The slightly greater capacitances of
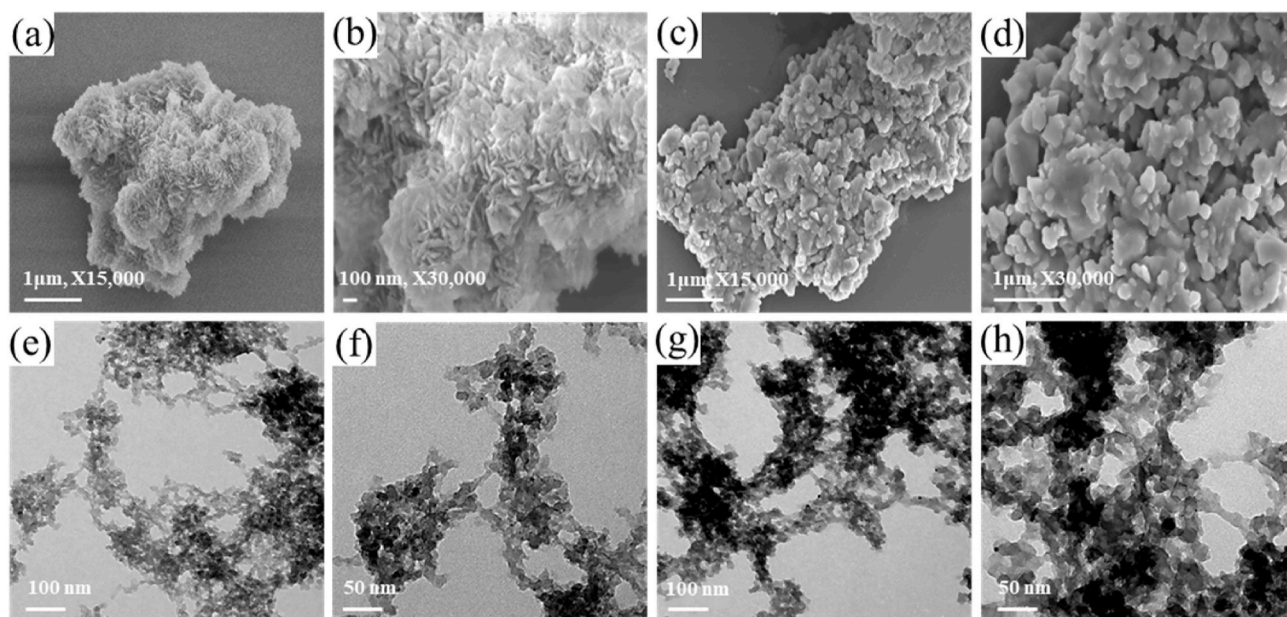
Fig. 4. FE-SEM images of BC-Py-CMP (a, b) and BC-BF-CMP (c, d). TEM images of BC-Py-CMP (e, f) and BC-BF-CMP (g, h), recorded at various magnifications.
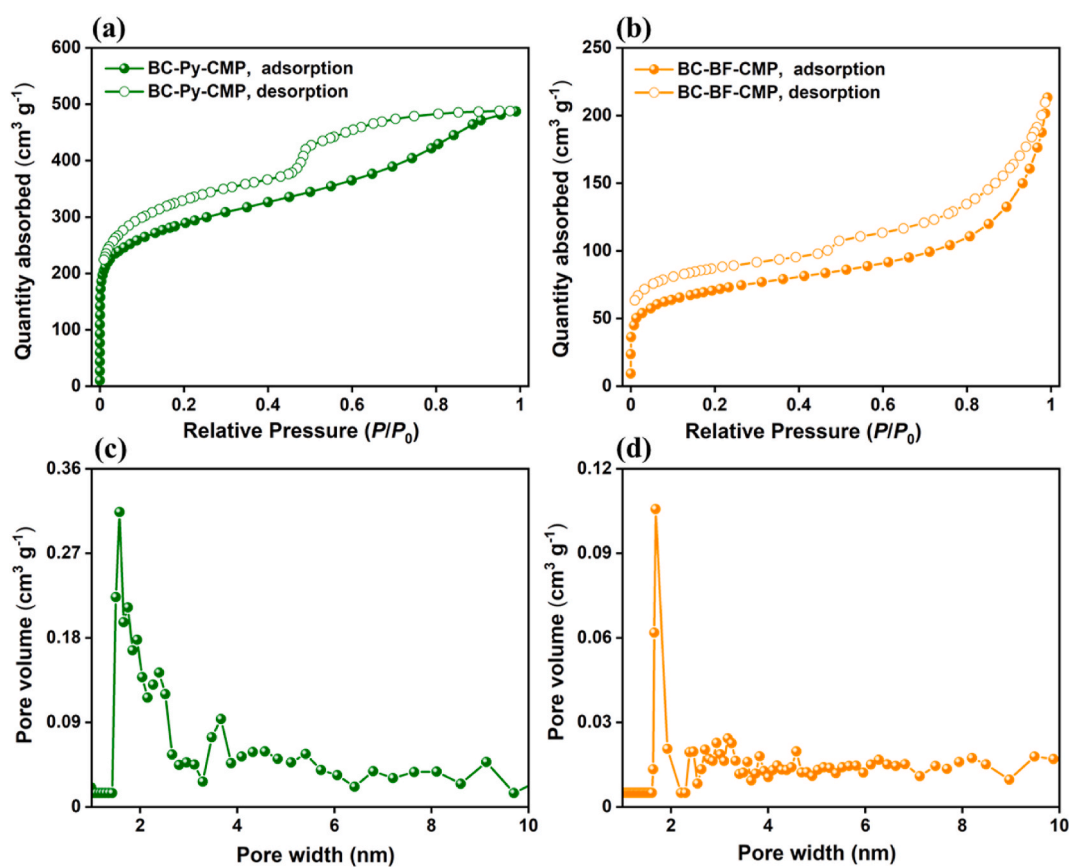

Fig. 5. N₂ adsorption and desorption isotherms of BC-Py-CMP (a, olive) and BC-BF-CMP (b, orange) recorded at 77K. Pore size distributions of BC-Py-CMP (c, olive) and BC-BF-CMP (d, orange) calculated using NLDFT. (For interpretation of the references to colour in this figure legend, the reader is referred to the Web version of this article.)

the BC-BF-CMP relative to those of the BC-Py-CMP were presumably due to the 9,9′-BF could easily accept one electron, causing the reduced form acquiring greater aromaticity by meeting Huckel's requirements, as a result improving the electron transporting properties [72]. The high electrochemical performance of BC-Py-CMP and BC-BF-CMP can attribute to their high surface areas (BC-Py-CMP: 1030 m² g⁻¹; BC-BF-CMP: 355 m² g⁻¹) and high pore volumes (BC-Py-CMP: 0.75 cm³ g⁻¹; BC-BF-CMP: 0.32 cm³ g⁻¹) as well as the presence of the electron-rich
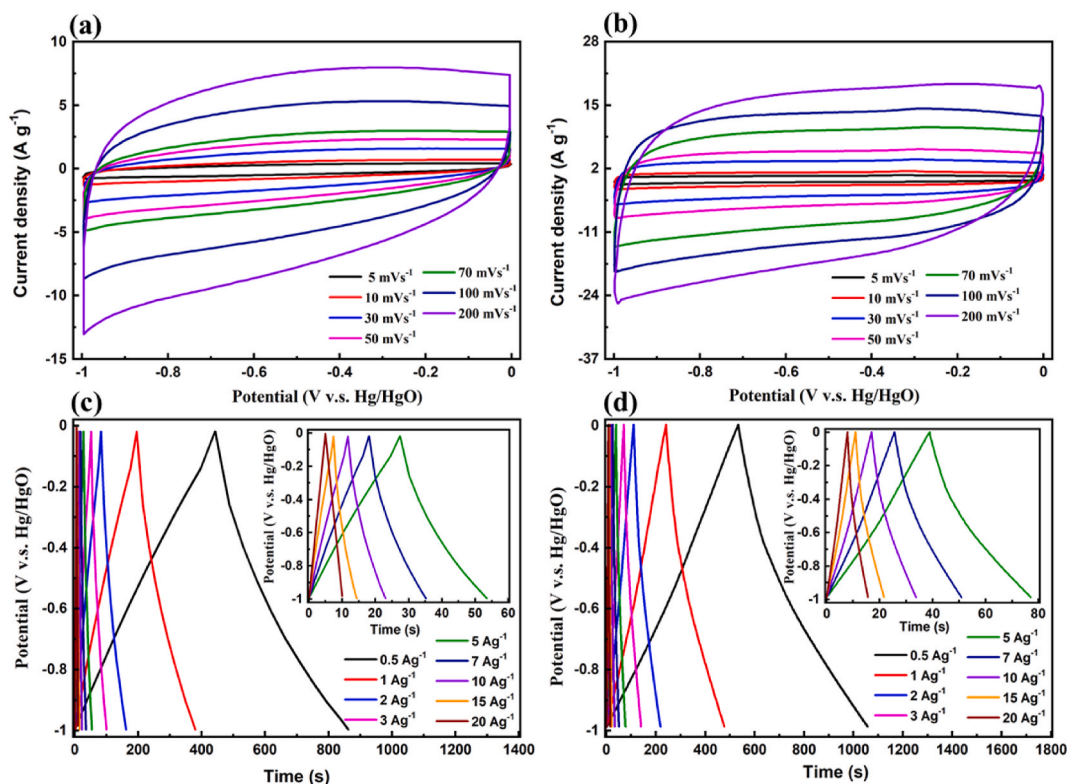
Fig. 6. Cyclic voltammetry curves of the (a) BC-Py-CMP and (b) BC-BF-CMP at various scan rates (mV s^{-1}). Galvanostatic charge-discharge curves of the (c) BC-Py-CMP and (d) BC-BF-CMP at various current densities (A g^{-1}).
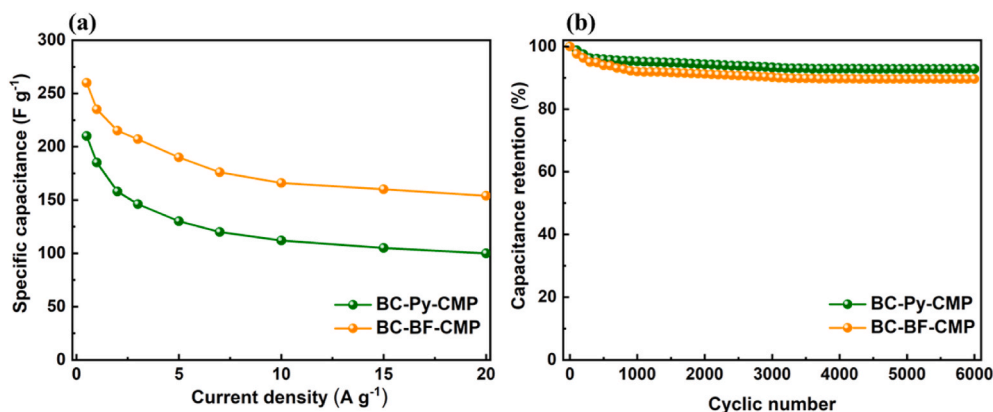

Fig. 7. Specific capacitances of the BC-Py-CMP (a, olive) and BC-BF-CMP (a, orange) electrodes at various current densities (A g^{-1}). Cycling performance of the BC-Py-CMP (b, olive) and BC-BF-CMP (b, orange) electrodes recorded at a current density of 2 A g^{-1}. (For interpretation of the references to colour in this figure legend, the reader is referred to the Web version of this article.)

BC, Py and 9,9′-BF units in their skeletons, all of which improved the electron transporting properties. BC-Py-CMP and BC-BF-CMP displayed specific capacitances higher than the values observed with other porous materials such as triethynylbenzene CMP (72 F g^{-1}), ferrocene-based (Fc)-CMP (147 F g^{-1}), pure reduced graphene oxide (rGO) (193 F g^{-1}) [73], MnO$_2$/Carbon-5 (164 F g^{-1}), MnO$_2$/Carbon-120 (218 F g^{-1}), MnO$_2$/Carbon-240 (166 F g^{-1}) [59], graphene hydrogel (GH)-CMP (206 F g^{-1}) [74], anthraquinone-based hyper-crosslinked porous organic polymers (72.75–98.4 F g^{-1}) [75], N-doped microporous carbon (185 F g^{-1}) [11], and covalent organic frameworks (0.24–51.3 F g^{-1}) [6] (Table 1). Some porous materials, however, have higher values such as CMP grafted on carbon nanotube fibers (670–751 mF cm^{-1}), and nitrogen-doped carbon aerogels (179–300 F g^{-1}). However, such materials were prepared through carbonization and multistep routes, in addition to the combination with highly conductive carbon nanotube fibers [76,77]. Recently, anthraquinone-based CMPs, namely poly-aminoanthraquinone (PAQ) networks have been prepared and featured specific capacitance values of 165–576 F g^{-1} [78]. Nitrogen-doped porous carbons were derived from the pyridyl- and triphenylamine conjugated microporous polytriphenylamine and exhibited a specific capacitance value up to 241 F g^{-1} [79]. Moreover, the conjugated microporous polymers formed through the polycondensation of 2,5-dia-minopyridine dihydrochloride and tris(4-bromo)phenylamine has been prepared and exhibited a specific capacitance value up 335 F g^{-1} [80]. Cycled over 6000 times at 2 A g^{-1} was used to determine the durability of these two CMPs samples (Fig. 7b). Both the BC-Py-CMP and BC-BF-CMP displayed outstanding cycling stability, having 92.42 and 89.60% retention, respectively, of their authentic capacitances after

Table 1

Comparison between the specific surface area/specific capacitance of BC-BF-CMP and BC-Py-CMP with those of previously reported materials for supercapacitor application.

COFs	S_{BET} (m² g⁻¹)	Capacitance	Electrolyte	Ref.
BC-BF-CMP	355	260 F g⁻¹ at 0.5 A g⁻¹	1.0 M KOH	This work
BC-Py-CMP	1030	211 F g⁻¹ at 0.5 A g⁻¹	1.0 M KOH	This work
Fc-CMPs	653.2	147 F g⁻¹ at 0.5 A g⁻¹	1.0 M H₂SO₄	73
rGO	–	193 F g⁻¹ at 0.5 A g⁻¹	1.0 M H₂SO₄	73
CMPs	672.3	72 F g⁻¹ at 0.5 A g⁻¹	1.0 M H₂SO₄	73
MnO₂/Carbon-5	–	164 F g⁻¹ at 0.1 A g⁻¹	1.0 M Na₂SO₄	59
MnO₂/Carbon-120	–	218 F g⁻¹ at 0.1 A g⁻¹	1.0 M Na₂SO₄	59
MnO₂/Carbon-240	–	166 F g⁻¹ at 0.1 A g⁻¹	1.0 M Na₂SO₄	59
GH-CMP	219	206 F g⁻¹ at 0.5 A g⁻¹	1.0 M H₂SO₄	74
An-CPOP-1	580	72.75 F g⁻¹ at 0.5 A g⁻¹	1.0 M KOH	75
An-CPOP-2	1130	98.4 F g⁻¹ at 0.5 A g⁻¹	1.0 M KOH	75
N-DMC	1469	185 F g⁻¹ at 1.0 A g⁻¹	1.0 M KCl	11
TPA–COF–1	714	51.3 F g⁻¹ at 0.2 A g⁻¹	0.5 M H₂SO₄	6
TPA–COF–2	478	14.4 F g⁻¹ at 0.2 A g⁻¹	0.5 M H₂SO₄	6
TPA–COF–3	557	5.1 F g⁻¹ at 0.2 A g⁻¹	0.5 M H₂SO₄	6
TPT–COF–4	1132	2.4 F g⁻¹ at 0.2 A g⁻¹	0.5 M H₂SO₄	6
TPT–COF–5	1747	0.34 F g⁻¹ at 0.2 A g⁻¹	0.5 M H₂SO₄	6
TPT–COF–6	1535	0.24 F g⁻¹ at 0.2 A g⁻¹	0.5 M H₂SO₄	6
CNF@PTPA1	123.64	751 mF cm⁻² at 1 mA cm⁻²	PVA/H₃PO₄	77
CNF@PTPA3	52.88	670 mF cm⁻² at 1 mA cm⁻²	PVA/H₃PO₄	76
NCA-700	615	179 F g⁻¹ at 0.5 A g⁻¹	1.0 M H₂SO₄	77
NCA-800	913	300 F g⁻¹ at 0.5 A g⁻¹	1.0 M H₂SO₄	77
NCA-900	1541	270 F g⁻¹ at 0.5 A g⁻¹	1.0 M H₂SO₄	77
NCA-1000	2356	222 F g⁻¹ at 0.5 A g⁻¹	1.0 M H₂SO₄	77
PAQTA	331	576 F g⁻¹ at 1.0 A g⁻¹	0.5 M H₂SO₄	78
PAQTB	600	165 F g⁻¹ at 1.0 A g⁻¹	0.5 M H₂SO₄	78
PAQCB	370	210 F g⁻¹ at 1.0 A g⁻¹	0.5 M H₂SO₄	78
PAQTM	545	208 F g⁻¹ at 1.0 A g⁻¹	0.5 M H₂SO₄	78
PAQSF	354	208 F g⁻¹ at 1.0 A g⁻¹	0.5 M H₂SO₄	78
NC-800	786	241 F g⁻¹ at 0.5 A g⁻¹	0.5 M H₂SO₄	79
PTPA-25	33	335 F g⁻¹ at 0.5 A g⁻¹	1.0 M H₂SO₄	80

6000 cycles.

4. Conclusions

We have prepared two carbazole-tethered conjugated microporous polymers, BC-Py-CMP and BC-BF-CMP, through the coupling reaction of the novel BC-4Bpin with Py-4Br and BF-4Br, respectively. We have utilized FTIR and solid state NMR spectroscopy to confirm the chemical structure of these CMPs, which featured outstanding thermal stabilities that reached up to T_{d10} value of approximately 694 °C and char yields of 85.50%. In addition, the synthesized CMPs exhibited high BET surface areas reached up to 1030 m² g⁻¹. The strut length of linker strongly controlled the BET specific surface areas of the resultant CMPs: the surface area increased upon the linker strut length decreased. Moreover, we have tested the synthesized CMPs for the energy storage application. the as-prepared BC-BF-CMP exhibited a high specific capacitance of 260 F g⁻¹ at 0.5 A g⁻¹ and showed outstanding cycling stability, having 89.60% capacitance retention of its authentic capacitance over 6000 cycles. As a result, it is a potential material for energy storage applications. The excellent electrochemical capacitances of the BC-BF-CMP were presumably due to the 9,9′-BF could easily accept one electron, causing the reduced form acquiring greater aromaticity by meeting Huckel's requirements, as a result improving the electron transporting properties.

CRediT authorship contribution statement

Mostafa Ahmed: Writing – original draft, Methodology, Data curation, Conceptualization. **Mohammed G. Kotp:** Writing – original draft, Investigation, Data curation, Conceptualization. **Tharwat Hassan Mansoure:** Methodology, Investigation, Data curation, Conceptualization. **Rong-Ho Lee:** Methodology, Investigation, Data curation, Conceptualization. **Shiao-Wei Kuo:** Writing – review & editing, Methodology, Data curation, Conceptualization. **Ahmed F.M. EL-Mahdy:** Writing – review & editing, Project administration, Methodology, Investigation, Data curation, Conceptualization.

Declaration of competing interest

The authors declare that they have no known competing financial interests or personal relationships that could have appeared to influence the work reported in this paper.

Acknowledgements

Appendix A. Supplementary data

Supplementary data to this article can be found online at https://doi.org/10.1016/j.micromeso.2022.111766.

References

[1] K.S.W. Sing, Reporting physisorption data for gas/solid systems with special reference to the determination of surface area and porosity (recommendations 1984), Pure Appl. Chem. 57 (1985) 603–619.
[2] A.P. Cote, A.I. Benin, N.W. Ockwig, M. O'Keeffe, A.J. Matzger, O.M. Yaghi, Porous, crystalline, covalent organic frameworks, Science 310 (2005) 1166–1170.
[3] J. Wu, F. Xu, S. Li, P. Ma, X. Zhang, Q. Liu, R. Fu, D. Wu, Porous polymers as multifunctional material platforms toward task-specific applications, Adv. Mater. 31 (2019) 1802922.
[4] J.W. Colson, W.R. Dichtel, Rationally synthesized two-dimensional polymers, Nat. Chem. 5 (2013) 453–465.
[5] X. Feng, X. Ding, D. Jiang, Covalent organic frameworks, Chem. Soc. Rev. 41 (2012) 6010–6022.
[6] A.F.M. El-Mahdy, C.-H. Kuo, A. Alshehri, C. Young, Y. Yamauchi, J. Kim, S.-W. Kuo, Strategic design of triphenylamine- and triphenyltriazine-based two-dimensional covalent organic frameworks for CO₂ uptake and energy storage, J. Mater. Chem. A 6 (2018) 19532–19541.
[7] A.F.M. El-Mahdy, C. Young, J. Kim, J. You, Y. Yamauchi, S.-W. Kuo, Hollow microspherical and microtubular [3+ 3] carbazole-based covalent organic frameworks and their gas and energy storage applications, ACS Appl. Mater. Interfaces 11 (2019) 9343–9354.
[8] Y.Z. Zhang, T. Cheng, Y. Wang, W.Y. Lai, H. Pang, W. Huang, A simple approach to boost capacitance: flexible supercapacitors based on manganese oxides@MOFs via chemically induced in situ self-transformation, Adv. Mater. 28 (2016) 5242–5248.
[9] Z. Liang, T. Qiu, S. Gao, R. Zhong, R. Zou, Multi-scale design of metal–organic framework-derived materials for energy electrocatalysis, Adv. Energy Mater. 12 (2021) 2003410.
[10] M.G. Mohamed, A.F.M. EL-Mahdy, Y. Takashi, S.-W. Kuo, Ultrastable conductive microporous covalent triazine frameworks based on pyrene moieties provide high-performance CO₂ uptake and supercapacitance, New J. Chem. 44 (2020) 8241–8253.
[11] H.R. Abuzeid, A.F.M. EL-Mahdy, M.M. Ahmed, S.-W. Kuo, Triazine-functionalized covalent benzoxazine framework for direct synthesis of N-doped microporous carbon, Polym. Chem. 10 (2019) 6010–6020.
[12] J. Du, Y. Zhang, H. Wu, S. Hou, A. Chen, N-Doped hollow mesoporous carbon spheres by improved dissolution-capture for supercapacitors, Carbon 156 (2020) 523–528.
[13] M. He, X. Ou, Y. Wang, Z. Chen, D. Li, B. Chen, B. Hu, Porous organic frameworks-based (micro) extraction, J. Chromatogr., A 1609 (2020) 460477.
[14] S. Ravi, Y. Choi, J.K. Choe, Novel phenyl-phosphate-based porous organic polymers for removal of pharmaceutical contaminants in water, Chem. Eng. J. 379 (2020) 122290.
[15] A. Foulet, M. Birot, G. Sonnemann, H. Deleuze, Life cycle assessment of producing emulsion-templated porous materials from kraft black liquor–comparison of a vegetable oil and a petrochemical solvent, J. Clean. Prod. 91 (2015) 180–186.
[16] L. Tiggemann, S.C. Ballen, C.M. Bocalon, A.M. Graboski, A. Manzoli, J. Steffens, E. Valduga, C. Steffens, Electronic nose system based on polyaniline films sensor

array with different dopants for discrimination of artificial aromas, Innovat. Food Sci. Emerg. Technol. 43 (2017) 112–116.

[17] J. Zou, A. Trewin, T. Ben, S. Qiu, High uptake and fast transportation of LiPF₆ in a porous aromatic framework for solid-state Li-ion batteries, Angew. Chem. 132 (2020) 779–784.

[18] A.F.M. EL-Mahdy, M.G. Mohamed, T.H. Mansoure, H.-H. Yu, T. Chen, S.-W. Kuo, Ultrastable tetraphenyl-p-phenylenediamine-based covalent organic frameworks as platforms for high-performance electrochemical supercapacitors, Chem. Commun. 55 (2019) 14890–14893.

[19] A.F.M. El-Mahdy, Y.H. Hung, T.H. Mansoure, H.H. Yu, T. Chen, S.W. Kuo, A hollow microtubular triazine- and benzobisoxazole-based covalent organic framework presenting sponge-like shells that functions as a high-performance supercapacitor, Chem. Asian J. 14 (2019) 1429–1435.

[20] A. Mukhtar, S. Saqib, N.B. Mellon, S. Rafiq, M. Babar, S. Ullah, N. Muhammad, A. L. Khan, M. Ayoub, M. Ibrahim, K. Maqsood, M.A. Bustam, A.G. Al-Sehemi, J. J. Klemeš, S. Asif, A. Bokhari, A Review on CO₂ capture via nitrogen-doped porous polymers and catalytic conversion as a feedstock for fuels, J. Clean. Prod. 277 (2020) 123999.

[21] D. Taylor, S.J. Dalgarno, Z. Xu, F. Vilela, Conjugated porous polymers: incredibly versatile materials with far-reaching applications, Chem. Soc. Rev. 49 (2020) 3981–4042.

[22] B. Singh, A. Kumar, Rohit, Synthesis and characterization of alginate and sterculia gum based hydrogel for brain drug delivery applications, Int. J. Biol. Macromol. 148 (2020) 248–257.

[23] M.G. Mohamed, C.-C. Lee, A.F.M. EL-Mahdy, J. Lüder, M.-H. Yu, Z. Li, Z. Zhu, C. C. Chueh, S.-W. Kuo, Exploitation of two-dimensional conjugated covalent organic frameworks based on tetraphenylethylene with bicarbazole and pyrene units and applications in perovskite solar cells, J. Mater. Chem. A 8 (2020) 11448–11459.

[24] J. Kang, S. Huang, K. Jiang, C. Lu, Z. Chen, J. Zhu, C. Yang, A. Ciesielski, F. Qiu, X. Zhuang, 2D porous polymers with sp²-carbon connections and sole sp²-carbon skeletons, Adv. Funct. Mater. 30 (2020) 2000857.

[25] A.F.M. EL-Mahdy, M.B. Zakaria, H.-X. Wang, T. Chen, Y. Yamauchi, S.-W. Kuo, Heteroporous bifluorenylidene-based covalent organic frameworks displaying exceptional dye adsorption behavior and high energy storage, J. Mater. Chem. A 8 (2020) 25148–25155.

[26] A.F.M. EL-Mahdy, T.-E. Liu, S.-W. Kuo, Direct synthesis of nitrogen-doped mesoporous carbons from triazine-functionalized resol for CO₂ uptake and highly efficient removal of dyes, J. Hazard Mater. 391 (2020) 122163.

[27] H.R. Abuzeid, A.F.M. EL-Mahdy, S.-W. Kuo, Covalent organic frameworks: design principles, synthetic strategies, and diverse applications, Gaint 6 (2021) 100054.

[28] J.X. Jiang, F. Su, A. Trewin, C.D. Wood, N.L. Campbell, H. Niu, C. Dickinson, A. Y. Ganin, M.J. Rosseinsky, Y.Z. Khimyak, A.I. Cooper, Conjugated microporous poly (aryleneethynylene) networks, Angew. Chem. Int. Ed. 46 (2007) 8574–8578.

[29] L. Li, Z. Cai, Q. Wu, W.-Y. Lo, N. Zhang, L.X. Chen, L. Yu, Rational design of porous conjugated polymers and roles of residual palladium for photocatalytic hydrogen production, J. Am. Chem. Soc. 138 (2016) 7681–7686.

[30] J.-S.M. Lee, A.I. Cooper, Advances in conjugated microporous polymers, Chem. Rev. 120 (2020) 2171–2214.

[31] Z. Qian, K.A.I. Zhang, Recent advances of conjugated microporous polymers in visible light–promoted chemical transformations, Solar RRL 5 (2020) 2000489.

[32] Y. Xu, S. Jin, H. Xu, A. Nagai, D. Jiang, Conjugated microporous polymers: design, synthesis and application, Chem. Soc. Rev. 42 (2013) 8012–8031.

[33] A.I. Cooper, Conjugated microporous polymers, Adv. Mater. 21 (2009) 1291–1295.

[34] J. Schmidt, M. Werner, A. Thomas, Conjugated microporous polymer networks via Yamamoto polymerization, Macromolecules 42 (2009) 4426–4429.

[35] J. Weber, A. Thomas, Toward stable interfaces in conjugated polymers: microporous poly(p-phenylene) and poly(phenyleneethynylene) based on a spirobifluorene building block, J. Am. Chem. Soc. 130 (2008) 6334–6335.

[36] J. Liu, J.M. Tobin, Z. Xu, F. Vilela, Facile ynthesis of a conjugated microporous polymeric monolith via copper-free Sonogashira–Hagihara cross-coupling in water under aerobic conditions, Polym. Chem. 6 (2015) 7251–7255.

[37] S. Yuan, B. Dorney, D. White, S. Kirklin, P. Zapol, L. Yu, D.-J. Liu, Microporous polyphenylenes with tunable pore size for hydrogen storage, Chem. Commun. 46 (2010) 4547–4549.

[38] C. Zhao, Z. Chen, R. Shi, X. Yang, T. Zhang, Recent advances in conjugated polymers for visible-light-driven water splitting, Adv. Mater. 32 (2020) 1907296.

[39] A.M. Elewa, M.H. Elsayed, A.F.M. EL-Mahdy, C.-L. Chang, L.-Y. Ting, W.-C. Lin, H.-H. Chou, Triptycene-based discontinuously-conjugated covalent organic polymer photocatalysts for visible-light-driven hydrogen evolution from water, Appl. Catal. B Environ. 285 (2020) 119802.

[40] S. Yuan, S. Kirklin, B. Dorney, D.-J. Liu, L. Yu, Nanoporous polymers containing stereocontorted cores for hydrogen storage, Macromolecules 42 (2009) 1554–1559.

[41] F. Bekkar, F. Bettahar, I. Moreno, R. Meghabar, M. Hamadouche, E. Hernáez, J.L. V. Vilela, L. Ruiz-Rubio, Polycarbazole and its derivatives: synthesis and applications. a review of the last 10 years, Polymers 12 (2020) 2227.

[42] Q. Chen, M. Luo, P. Hammershøj, D. Zhou, Y. Han, B.W. Laursen, C.G. Yan, B.-H. Han, Microporous polycarbazole with high specific surface area for gas storage and separation, J. Am. Chem. Soc. 134 (2012) 6084–6087.

[43] X. Liu, Y. Xu, D. Jiang, Conjugated microporous polymers as molecular sensing devices: microporous architecture enables rapid response and enhances sensitivity in fluorescence-on and fluorescence-off sensing, J. Am. Chem. Soc. 134 (2012) 8738–8741.

[44] K. Rakstys, S. Paek, A. Drevilkauskaite, H. Kanda, S. Daskeviciute, N. Shibayama, M. Daskeviciene, A. Gruodis, E. Kamarauskas, V. Jankauskas, V. Getautis, M.

[45] K. Nazeeruddin, Carbazole-terminated isomeric hole-transporting materials for perovskite solar cells, ACS Appl. Mater. Interfaces 12 (2020) 19710–19717.

[45] R. Yu, P. Wang, X. Meng, L. He, Sky-blue-emitting cationic iridium complexes with carbazole-type counter-anions and their use for efficient solution-processed organic light-emitting diodes, Dalton Trans. 49 (2020) 8967–8975.

[46] T. Ishi-i, H. Tanaka, I.S. Park, T. Yasuda, S.-I. Kato, M. Ito, H. Hiyoshi, T. Matsumoto, White-light emission from a pyrimidine–carbazole conjugate with tunable phosphorescence–fluorescence dual emission and multicolor emission switching, Chem. Commun. 56 (2020) 4051–4054.

[47] A.F.M. EL-Mahdy, Y.H. Hung, T.H. Mansoure, H.-H. Yu, Y.-S. Hsu, K.C.W. Wu, S.-W. Kuo, Synthesis of [3+ 3] β-ketoenamine-tethered covalent organic frameworks (COFs) for high-performance supercapacitance and CO₂ storage, J. Taiwan Inst. Chem. Eng. 103 (2019) 199–208.

[48] T. Nishimoto, T. Yasuda, S.Y. Lee, R. Kondo, C. Adachi, A six-carbazole-decorated cyclophosphazene as a host with high triplet energy to realize efficient delayed-fluorescence OLEDs, Mater. Horiz. 1 (2014) 264–269.

[49] A.F.M. EL-Mahdy, A.M. Elewa, S.W. Huang, H.H. Chou, S.W. Kuo, Dual-function fluorescent covalent organic frameworks: HCl sensing and photocatalytic H₂ evolution from water, Adv. Opt. Mater. 8 (2020) 2000641.

[50] A.F.M. EL-Mahdy, M.-Y. Lai, S.-W. Kuo, A highly fluorescent covalent organic framework as a hydrogen chloride sensor: roles of schiff base bonding and π-stacking, J. Mater. Chem. C 8 (2020) 9520–9528.

[51] G. Bagdžiūnas, D. Palinauskas, Poly(9H-Carbazole) as a organic semiconductor for enzymatic and non-enzymatic glucose sensors, Biosensors 10 (2020) 104.

[52] H.R. Abuzeid, A.F.M. EL-Mahdy, S.-W. Kuo, Hydrogen bonding induces dual porous types with microporous and mesoporous covalent organic frameworks based on bicarbazole units, Microporous Mesoporous Mater. 300 (2020) 110151.

[53] R. Rojaee, R. Shahbazian-Yassar, Two-dimensional materials to address the lithium battery challenges, ACS Nano 14 (2020) 2628–2658.

[54] S. Dutta, J. Kim, Y. Ide, J.H. Kim, M.S.A. Hossain, Y. Bando, Y. Yamauchi, K.C.-W. Wu, 3D network of cellulose-based energy storage devices and related emerging applications, Mater. Horiz. 4 (2017) 522–545.

[55] V. Veeramani, M. Sivakumar, S.-M. Chen, R. Madhu, H.R. Alamri, Z.A. Alothman, M.S.A. Hossain, C.K. Chen, Y. Yamauchi, N. Miyamoto, K.C.-W. Wu, Lignocellulosic biomass-derived, graphene sheet-like porous activated carbon for electrochemical supercapacitor and catechin sensing, RSC Adv. 7 (2017) 45668–45675.

[56] R.R. Salunkhe, J. Wang, A. Alowasheeir, J. Lin, V. Malgras, Y. Bando, M.B. Zakaria, A.A. Alshehri, J. Kim, Y. Yamauchi, K.C.W. Wu, Three-dimensional macroporous graphitic carbon for supercapacitor application, ChemistrySelect 3 (2018) 4522–4526.

[57] A.F.M. EL-Mahdy, T.C. Yu, M.G. Mohamed, S.-W. Kuo, Secondary structures of polypeptide-based diblock copolymers influence the microphase separation of templates for the fabrication of microporous carbons, Macromolecules 54 (2020) 1030–1042.

[58] G. Wang, L. Zhang, J. Zhang, A review of electrode materials for electrochemical supercapacitors, Chem. Soc. Rev. 41 (2012) 797–828.

[59] Y. Peng, Z. Chen, J. Wen, Q. Xiao, D. Weng, S. He, H. Geng, Y. Lu, Hierarchical manganese oxide/carbon nanocomposites for supercapacitor electrodes, Nano Res. 4 (2011) 216–225.

[60] A.M. Khattak, H. Yin, Z.A. Ghazi, B. Liang, A. Iqbal, N.A. Khan, Y. Gao, L. Li, Z. Tang, Three dimensional iron oxide/graphene aerogel hybrids as all-solid-state flexible supercapacitor electrodes, RSC Adv. 6 (2016) 58994–59000.

[61] I.E. Rauda, V. Augustyn, B. Dunn, S.H. Tolbert, Enhancing pseudocapacitive charge storage in polymer templated mesoporous materials, Acc. Chem. Res. 46 (2013) 1113–1124.

[62] A.M. Khattak, H. Sin, Z.A. Ghazi, X. He, B. Liang, N.A. Khan, H.R. Alanagh, A. Iqbal, L. Li, Z. Tang, Controllable fabrication of redox-active conjugated microporous polymers on reduced graphene oxide for high performance faradaic energy storage, J. Mater. Chem. A 6 (2018) 18827–18832.

[63] H. Nishihara, T. Kyotani, Templated nanocarbons for energy storage, Adv. Mater. 24 (2012) 4473–4498.

[64] P. Simon, Y. Gogotsi, Nanoscience and Technology: a collection of reviews from, Nat. J. World Sci. (2010) 320–329.

[65] A.F.M. EL-Mahdy, T.C. Yu, S.-W. Kuo, Synthesis of multiple heteroatom–doped mesoporous carbon/silica composites for supercapacitors, Chem. Eng. J. 414 (2021) 128796.

[66] H. Li, W. Lyu, Y. Liao, Engineering redox activity in conjugated microporous polytriphenylamine networks using pyridyl building blocks toward efficient supercapacitors, Macromol. Rapid Commun. 40 (2019) 1900455.

[67] A.C. Lim, H.S. Jadhav, J.G. Seo, Electron transport shuttle mechanism via an Fe–N–C bond derived from a conjugated microporous polymer for a supercapacitor, Dalton Trans. 47 (2018) 852–858.

[68] Y.G. Wang, H.Q. Li, Y.Y. Xia, Ordered whiskerlike polyaniline grown on the surface of mesoporous carbon and its electrochemical capacitance performance, Adv. Mater. 18 (2006) 2619–2623.

[69] S. Hayashi, Y. Togawa, S.I. Yamamoto, T. Koizumi, K. Nishi, A. Asano, Synthesis of π-conjugated network polymers based on fluoroarene and fluorene units via direct arylation polycondensation and their porosity and fluorescent properties, J. Polym. Sci., Part A: Polym. Chem. 55 (2017) 3862–3867.

[70] J.X. Jiang, F. Su, A. Trewin, C.D. Wood, H. Niu, J.T.A. Jones, Y.Z. Khimyak, A. I. Cooper, Synthetic control of the pore dimension and surface area in conjugated microporous polymer and copolymer networks, J. Am. Chem. Soc. 130 (2008) 7710–7720.

[71] C. Su, H. He, L. Xu, K. Zhao, C. Zheng, C. Zhang, A mesoporous conjugated polymer based on a high free radical density polytriphenylamine derivative: its preparation

and electrochemical performance as a cathode material for Li-ion batteries, J. Mater. Chem. A. 5 (2017) 2701–2709.

[72] H.U. Kim, J.H. Kim, H. Suh, J. Kwak, D. Kim, A.C. Grimsdale, S.C. Yoon, D. H. Hwang, High open circuit voltage organic photovoltaic cells fabricated using 9,9'-bifluorenylidene as a non-fullerene type electron acceptor, Chem. Commun. 49 (2013) 10950–10952.

[73] A.M. Khattak, H. Sin, Z.A. Ghazi, X. He, B. Liang, N.A. Khan, H.R. Alanagh, A. Iqbal, L. Li, Z. Tang, Controllable fabrication of redox-active conjugated microporous polymers on reduced graphene oxide for high performance faradaic energy storage, J. Mater. Chem. A 6 (2018) 18827–18832.

[74] M. Zhang, T. Zhao, J. Dou, Z. Xu, W. Zhang, X. Chen, X. Wang, B. Zhou, Bottom-up construction of conjugated microporous polyporphyrin-coated graphene hydrogel composites with hierarchical pores for high-performance capacitors, Chemelectrochem 6 (2019) 5946–5950.

[75] M.G. Mohamed, X. Zhang, T.H. Mansoure, A.F.M. EL-Mahdy, C.-F. Huang, M. Danko, Z. Xin, S.-W. Kuo, Hypercrosslinked porous organic polymers based on tetraphenylanthraquinone for CO_2 uptake and high-performance supercapacitor, Polymer 205 (2020) 122857–122866.

[76] W. Lyu, W. Zhang, H. Liu, Y. Liu, H. Zuo, C. Yan, C.F. Faul, A. Thomas, M. Zhu, Y. Liao, Conjugated microporous polymer network grafted carbon nanotube fibers with tunable redox activity for efficient flexible wearable energy storage, Chem. Mater. 32 (2020) 8276–8285.

[77] H. Li, J. Li, A. Thomas, Y. Liao, Ultra-high surface area nitrogen-doped carbon aerogels derived from a schiff-base porous organic polymer aerogel for CO_2 storage and supercapacitors, Adv. Funct. Mater. 29 (2019) 1904785.

[78] Y. Liao, H. Wang, M. Zhu, A. Thomas, Efficient supercapacitor energy storage using conjugated microporous polymer networks synthesized from buchwald-hartwig coupling, Adv. Mater. 30 (2018) 1705710.

[79] N. Meng, H. Li, Y. Liu, Y. Liao, Self-templating synthesis of nitrogen-rich porous carbons using pyridyl functionalized conjugated microporous polytriphenylamine for electrochemical energy storage, Electrochim. Acta 402 (2022) 139531.

[80] H. Li, W. Lyu, Y. Liao, Engineering redox activity in conjugated microporous polytriphenylamine networks using pyridyl building blocks toward efficient supercapacitors, Macromol. Rapid Commun. 40 (2019) 1900455.